http://dx.doi.org/10.11142/jicems.2013.2.3.275

Fast Component Placement with Optimized Long-Stroke Passive Gravity Compensation Integrated in a Cylindrical/Tubular PM Actuator

J.J.H. Paulides *, L. Encica **, K.J. Meessen **, and E.A. Lomonova***

Abstract – Applications such as vibration isolation, gravity compensation, pick-and-place machines, etc., would benefit from (long-stroke) cylindrical/tubular permanent magnet (PM) actuators with integrated passive gravity compensation to minimize the power consumption. As an example, in component placing (pick-and-place) machines on printed circuit boards, passive devices allow the powerless counteraction of translator including nozzles or tooling bits. In these applications, an increasing demand is arising for high-speed actuation with high precision and bandwidth capability mainly due to the placement head being at the foundation of the motion chain, hence, a large mass of this device will result in high force/power requirements for the driving mechanism (i.e. an H-bridge with three linear permanent magnet motors placed in an H-configuration). This paper investigates a tubular actuator topology combined with passive gravity compensation. These two functionalities are separately introduced, where the combination is verified using comprehensive three dimensional (3D) finite element analyses.

Keywords: Component placement machines, Placement head, Pick-and-place, Electronics assembly equipment, Gravity compensation, Tubular actuator, Cylindrical actuator.

1. Introduction

In manufacturing automation, the most important performance requirements of robot manipulators for assembly of electronics parts are positioning accuracy, allowable component size and high accelerating motion. Limitations on these performance characteristics are imposed by mechanical design aspects such as structure, materials used in the linkage, mass distribution techniques and by the drive system components such as gearing, spindle screws and actuators. To overcome many of these limitations, direct-drive H-bridge robot manipulators are introduced to place large components onto PCBs (printed circuit board), as shown in Fig. 1.

The placement rate of these machines can be optimized by considering significant factors such as the placement head travel, the placement sequence and the position of components in the feeder bank. This machine assembles components onto a PCB, where in general, each machine has a feeder carrier (or magazine), a PCB table (or worktable), head(s), nozzle(s) (or gripper) and a tool magazine. The PCB table, the feeder carrier and the head can either be moveable or fixed. The feeder reels (tapes holding electronic components) are positioned in feeder slots. Most commonly, larger components are supplied by tray feeders. The components are transported from these feeders to the placement position on the PCB using vacuum nozzle(s) which are placed at the end of the head [1], as shown in Fig. 2.

Fig.1. Current AX-201 component mounter.

* Eindhoven University of Technology, Electromechanics and Power Electronics group, the Netherlands, w3.ele.tue.nl/nl/epe/ (j.j.h.paulides@tue.nl & e.lomonova@tue.nl)

** Advanced Electromagnetics BV, Kerkstraat 13, 5161EA Sprang-Capelle, the Netherlands, www.ae-grp.nl (laurentiu@ae-magnetics.nl)

*** Prodrive BV, Science Park Eindhoven 5501, 5692 EM Son, The Netherlands, www.prodrive.nl (koen.meessen@prodrive.nl)

Received 13 June 2013; Accepted 20 August 2013

More specifically, in the AX-201 component placement machine (www.assembleon.com) with the characteristics summarized in Table 1, the PCB is locked in position by a table which is also used to locate the required points for the placement operations. This PCB table uses a conveyor system and the placement heads are moved by an X-Y motion table, as shown in Fig. 2. This machine offers a combination of high placement accuracy and speed with an extremely wide component range. Therefore, it can be used for either stand-alone applications or as an end-of-line machine in combination with other component placement machines.

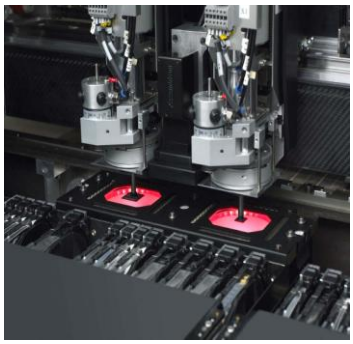

Fig.2. Current moving head which holds the components above camera's for identification (two pick-and-place devices are shown).

Table 1. Specifications AX-201 component mounter

Maximum output per hour	5300
IPC 9850 output per hour	3900
Placement accuracy (3s)	25 micron
Component rage	0.4*0.2mm/163*23mm
Maxmun component height	50mm
Maximun board size (L*W)	Standard 508*460mm
Tape feeding positions	96 (212(twin tape))

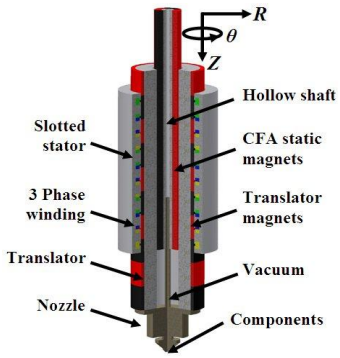

Fig.3. Linear part of the placement head consisting of a tubular permanent magnet actuator combined with a passive linear constant force actuator.

A lot of work has been done on improving the efficiency of component placement machines [2-4]. However, most previous work involves software improvements, e.g. an offline scheduler to reduce the number of component being missing from the feeder carrier. This paper presents a different approach, since there is an increasing demand for high-speed actuation with high precision and high bandwidth capability. As such, the most generic device of any component mounting machine is the placement head. This device is at the foundation of the motion chain and a large mass of this device will result in high force/power requirements for the H-bridge (three linear permanent magnet motors placed in an H-configuration, e.g., two for the y-axis movement and one for x-axis movement).

The complete pick-and-place action requires a four degrees-of-freedom robotic motion. This paper focuses on the short-stroke (50 mm) linear motion in the vertical direction to pick and place the components, as shown in Fig. 3. To increase the throughput of the total pick-and-place cycle a high force requirement of 300 N is needed to achieve the acceleration level with an added mass of 120 N.

In general, the linear Z-axis movement of the placement heads is augmented by a mechanical coil spring to ensure that the placement head cannot crash into the PCB when there is a power disruption or software failure. However, when moving downwards the linearly increasing spring force needs to be actively counteracted by the tubular actuator, which does result in a significant power demand. A more suitable solution would be provided by electromagnetic means, in such a manner that the mass of the translator, nozzle or gripper and average component can be passively compensated, estimated to be 120 N in this application. This can be achieved by combining the tubular permanent magnet (PM) actuator with a constant force actuator (CFA) as shown in Fig. 3, which results in a significant improvement of the dynamic behavior. As such, Section II discusses the used optimization routine, Section III the design of the tubular permanent magnet actuator, Section IV the constant force actuator design and Section V the combined actuator. Finally, Section VI provides the conclusions.

2. Optimization routine

Analytical determination of actuator performance provides an elegant way to design PM machines, e.g. lumped parameter model or analytical equations [5-9]. However, in order to implement these models certain assumptions need to be considered, hence, sometimes small model inaccuracies occur. For example, flux fringing, complex shapes, leakage, magnetic saturation, etc. are in general neglected although that significant progress is currently undertaken [10-11], which results in some small loss of accuracy. Therefore, numerical techniques are still

used to determine the field distribution and equivalent electric circuit components, especially for 3D structures. However, using solely finite element (FE) techniques is time demanding and therefore rather inefficient for design optimization.

An alternative method is given by the space mapping (SM) technique as introduced in [12]. This optimization technique is surrogate-based where a simple physics based (coarse) model is exploited and aligned with the computationally intensive accurate (fine) model. This technique has successfully been applied in the field of microwaves for component and system modeling [13]. In this paper, the tubular and constant force actuators have been optimized using the SM technique [14, 15]. The optimization routines together with the corresponding models are implemented in a Matlab (The MathWorks Inc.) and Maxwell 3D (Ansys) environment.

Tubular permanent magnet actuator optimization includes the selection of numerous dimensional and performance variables, e.g. pole pair, tooth thickness, tooth tip dimensions, winding configuration, slot number, pole-pitch, slot opening, coil-pitch, etc. In general, optimization routines primary design for high efficiency, however, also force density should be taken into account. In this optimization, therefore the translator mass has been included. Further, in slotted actuators, the winding and tooth area are contending for the same volume, hence, the magnetic and electrical loadings have been optimized by not only considering the magnetic parameters but also the thermal considerations.

The proposed design methodology has the following structure: an optimization problem is formulated for the proposed tubular actuator and an SM variant is implemented for determining the corresponding solution; the objective is the minimization of the actuator's mass while providing a specified (static) force response (100 N for a single pole pair) and limiting the levels of iron core flux densities and of generated heat through copper loss; corresponding magnetic and thermal models have been defined, where the tubular actuator optimization is summarized in the next Section, and, consequently, the CFA is optimized in Section IV. The combined actuator will be presented in Section V.

3. Tubular/Cylindrical PM Actuator

A slotted tubular PM actuator, as shown in Fig. 4, is particularly interesting as it has a high force density, no end-windings and zero net radial attraction force between the translator and armature. The tubular actuator consists of a stator and a translator, where the moving magnet actuator is preferred since it does not require connections to the moving part. The stator of the TPMA contains coils and is mostly either slotted or slotless, where the highest force density can be achieved when a slotted structure is used [5]. However, the slotted structure also has some disadvantages, e.g. the reluctance in the air gap is not uniform resulting in an extra force component called cogging force [16]. This can be minimized by introducing typical pole-slot combination, albeit this reduces the winding factor, and hence, the force capability. In this actuator skewing will be applied, which results in the actuator being suitable for this precision positioning application, hence, a smooth force versus position characteristic.

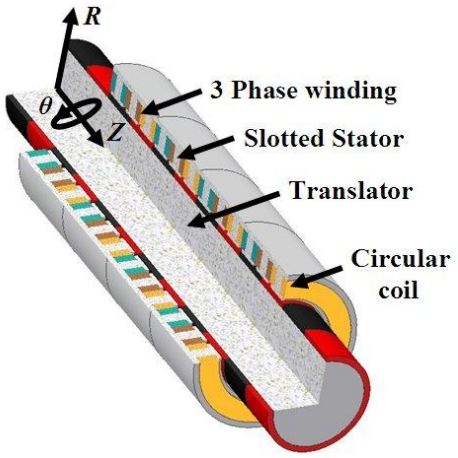

Fig.4. TPMA (axial cross-section of one pole-pair): topology and design variables.

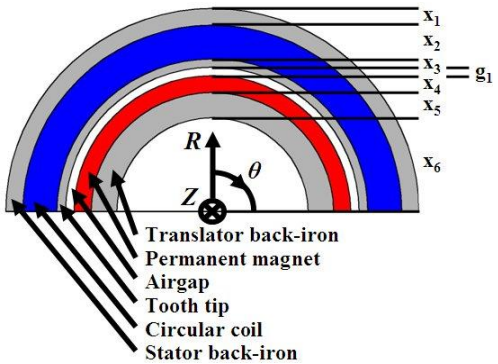

Fig.5. TPMA radial cross-section: topology and design variables.

As already mentioned in Section II, the design objective was to minimize the actuator mass for a specified force output. In addition, upper limits are imposed on the average flux density levels in the iron core and on the peak temperature. This optimization routine has been previously reported in [14], where the combined electromagnetic with thermal analysis is used as a basis for this paper. Therefore,

the TPMA radial cross-section is shown in Fig. 5 and axial in Fig. 6, respectively. The relative dimensions and design specifications (i.e. linear and nonlinear constraints), i.e. force output, the maximum admissible average flux densities in three regions of the iron core and the maximum admissible temperature, are summarized in Table 2.

The TPMA optimal design problem was solved considering a heat convection boundary condition with a value of 20 Wm-2K-1 specified on the outer lateral surface of the actuator, with an ambient temperature of 25 ℃. The magnetic flux density distribution is shown in Fig. 7. It must be noted that for this design the shaft material was not considered, and thus the shaft was not included in the total calculated mass.

Table 2. Design results and specifications

[x1,x2.x3] (mm)	[6.0,6.4,2.0]
[x4,x5,x6] (mm)	[5.0,15.2,23.7]
[x7,x8,x9,x10] (mm)	[1.8,5.5,3.6,29.6]
Airgap.g1 (mm)	1.0
Force (N)	100
Mean flux density back-iron (T)	1.3
Inner coil temperature (° C)	130

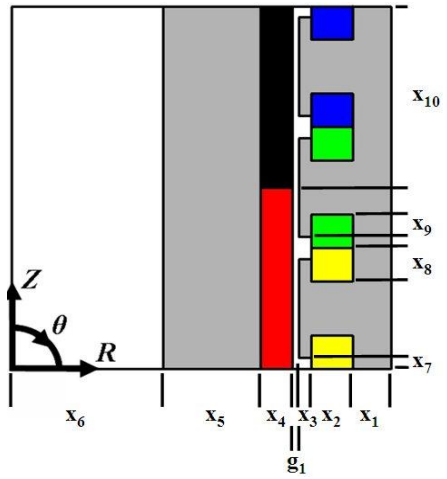

Fig. 6. TPMA axial cross-section: topology and design variables.

4. Optimal gravity compensator design

Passive gravity compensators (or constant force actuators) and their respectively force-displacement characteristics are discussed in [15, 17]. In general, this actuator is placed externally in parallel to the linear actuator. Further, no position sensor is required and an enhancement could be achieved if the given force characteristic could be varied by means of a predetermined constant current force-displacement actuator [17, 18]. For shorter strokes, couple of cm's or less, solenoids producing a force depending on current are used. These solenoids have a very simple structure and are therefore amenable to mass production. However they, in order to produce force, require a constant current excitation and usually still have to use a spring to return to their initial position. This paper, therefore, presents the optimal design of a long stroke constant force-displacement actuator topology, as shown in Fig. 3, that fits inside the tubular actuator with a constant passive (without energy consumption) force independent on the position for 90% of the stroke for a passive force level of 120 N, respectively.

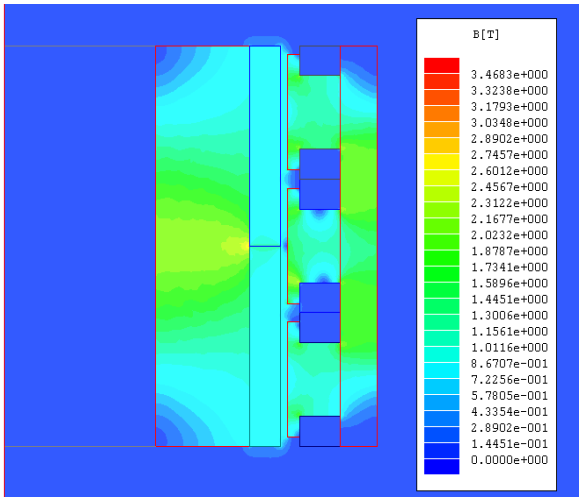

Fig. 7. TPMA – flux density distribution of lectromagnetic-thermal design solution.

Initially, the force capability of the constant force actuator can be derived from well-established analytical expressions. This simplified analytical model is derived based on the following assumptions:

- no leakage fluxes or fringing effects are considered, and
- the magnet and iron relative permeabilities are taken to be equal to 1 and ∞, respectively.

For a magnet material having a linear demagnetization characteristic, with a working point that lies on the linear region, the flux density is given by:

$$B_m = B_r + \mu_o \mu_r H_m \tag{1}$$

where, B_m is the working flux density, H_m is the corresponding magnetic field strength, B_r is the remanent flux density and μ_r is the relative recoil permeability.

Starting from the general form of Ampere's law:

$$\oint_C \bar{H} \cdot d\bar{l} = \iint_S \bar{J} \cdot d\bar{A} = I_{enc} \tag{2}$$

and considering the magnetic field strength to be (piece-

wise) constant on the integration path, the simplified expression is obtained:

$$H_g l_g + H_m l_m = 0 \tag{3}$$

Further, it is assumed that the airgap and magnet flux are equal. Hence, for the surface-mounted magnet rotor structure the average magnet flux density, from (1), is:

$$B_m = \frac{B_r}{1+\frac{l_g S_m}{l_m S_g}} \tag{4}$$

where lg and Sg are the airgap length and surface area, and lm and Sm are the magnet thickness and the magnet area, respectively. The airgap flux density can be derived from (5) as:

$$B_g = B_m \frac{S_m}{S_g} \tag{5}$$

The force is then derived from the rate of change of magnetic co-energy with respect to the translator displacement, where the force level, for the direction of travel along the z-axis, is then calculated by:

$$F_z = -\left.\frac{\partial W'}{\partial z}\right|_{I=const} \tag{6}$$

then, by substituting (4) and (5) in (6), the following expression, which is independent of the z-axis displacement due to the exclusion of axial leakage in the analytical model, can be obtained for the force amplitude:

$$F_z = -\frac{{B_r}^2}{2\mu_0} c_m l_m \left[\frac{1}{1+\frac{l_{g1} c_m}{l_m c_{g1}}} - \frac{1}{1+\frac{l_{g2} c_m}{l_m c_{g2}}} \right] \tag{7}$$

In this, c_g and c_m are the width of the airgap and magnet flux path, respectively, and the expressions for calculating the various parameters considered are summarized in Table 3. In this, l_{g1} and c_{g1} are, correspondently, the length and area of the airgap of the overlapping part, l_{g2} and c_{g2} are the length and airgap of the non-overlapping part and l_m and c_m are the length and area of the permanent magnets. The various dimensions of x_{11} to x_{14} and g_2 are shown in Fig. 8 and summarized in Table 4. Further, n_p represents the number of poles, where the use of a low number of poles in CFAs (typically 2-4) is implemented.

To increase the force level and density, the pole-pair number selection is significantly influenced by considerations regarding the size and leakage, since increasing the number of poles, reduces the stationary and translating back-iron thicknesses. However, it may also lead to a higher leakage flux, and thus, a decrease of the average airgap flux, hence, decreased forces. This is illustrated by Fig. 8, which shows the influence of varying the number of poles within the CFA. Clearly it can be seen that a reduced number of poles results in a smaller outer radius, hence, leakage flux is significant when the outer radius is relatively small. This also results in a smaller stator mass of the CFA, however a slight increased translator mass.

Table 3. Parameters for the passive CFA

l_{g1}	2g
c_{g1}	$2\pi\ (x_{11}+x_{12}+g_2/2)/n_p/2$
l_{g2}	$2\pi\ (x_{11}+x_{12}+g_2)/n_p/2$
c_{g2}	$2\pi\ (x_{11}+x_{12}+g_2)/n_p/2$
l_m	$2\ x_{13}$
c_m	$2\pi\ (x_{11}+x_{12}+g_2+x_{13}/2)/n_p/2$

Table 4. Constant force actuator parameters

	$n_p = 4$	$n_p = 6$	$n_p = 8$	$n_p = 10$
x_{11} (mm)	5.33	4.45	3.98	3.66
g_2 (mm)	1.0	1.0	1.0	1.0
x_{12} (mm)	8.65	8.75	9.04	9.32
x_{13} (mm)	4.26	3.56	3.18	2.93
x_{14} (mm)	3.37	7.08	10.21	13.02
Outer radius (mm)	22.61	24.83	27.41	29.94
Translator mass (kg)	1.02	0.96	0.97	0.99
Stator mass (kg)	1.23	1.57	1.93	2.27

The magnetic loading, B_r, determines the specific force capability, as it is clear from (10). Further, it seems that scaling the surface-mount magnets produces an increase in airgap flux density. However, if the airgap could be reduced a significantly smaller magnet thickness could provide the same force. Additionally an upper constraint could be implemented on the magnet thickness. Further, the CFA force output could also be varied by adding a stator mmf using a meandered wound coil in between the magnets, which allows for deviations of the constant force characteristic amplitude [12].

5. Combined actuator analysis

The combined tubular and constant force actuator topology requires a 3D representation, as shown in Fig. 10a, where the actuator is modeled in magneto-static 3D finite

element. However, this does require approximately 50,000 tetrahedra elements to achieve an accurate force response (for an active length of 198 mm Fig. 10b). By utilizing the symmetry inside the model this finite element model can be reduced to a quarter for the CFA of Fig. 8, as shown in Fig. 10a.

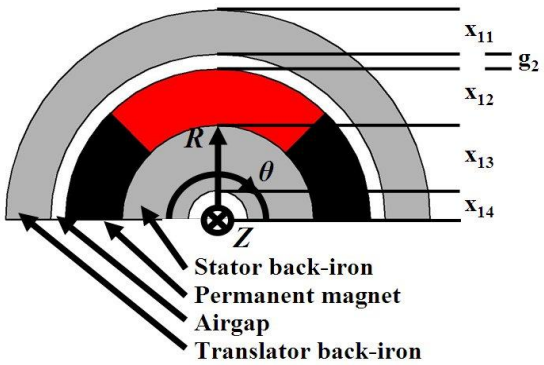

Fig. 8. CFA radial cross-section: topology and design variables.

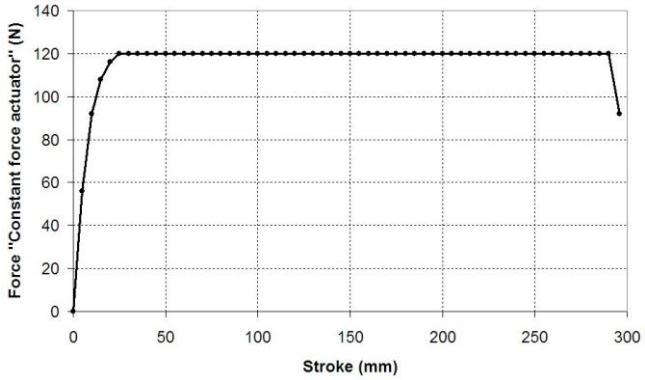

Fig. 9. CFA Force versus stroke characteristic.

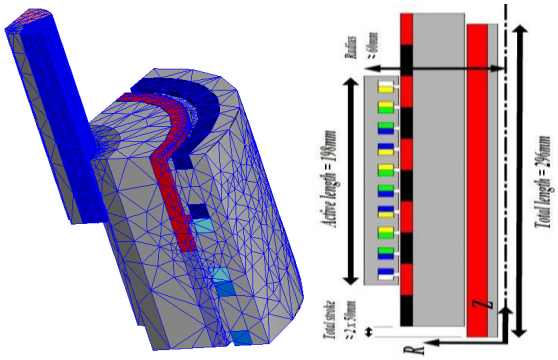

(a) (b)

Fig. 10. Combined tubular permanent magnet with constant force actuator (a) 3D finite element analyses (b) cross-section with overall parameters.

The relative evaluated dimensions and geometry are given by combining Tables 2 and 4. These dimensions are separately optimized designs combined into a single actuator. The permanent magnets are assumed to be a sintered NdFeB with a remanence of 1.23T and can be either radially or parallel magnetized. Further, the standard non-linear BH-curve for mild steel, AI 1010, is used for both stationary as translating back-iron.

The force-displacement characteristic of the combined actuator is shown in Fig. 10. In this figure a stroke of 0 mm (initial position) corresponds to the stator with magnets and translator of the CFA being fully aligned and Fig. 11 shows the resulting force characteristics. Using the 3D FE analyses, simulations at various positions of the CFA inner part (stator) have been undertaken, which results in the force acting on the combined translator is the sum of the TPMA (approximately 300 N), CFA (120 N) force and gravitational force responses, as shown in Fig. 11. This gives that the combined actuator allows for the compensation of a mass of some 120 N when moving downwards from the equilibrium position.

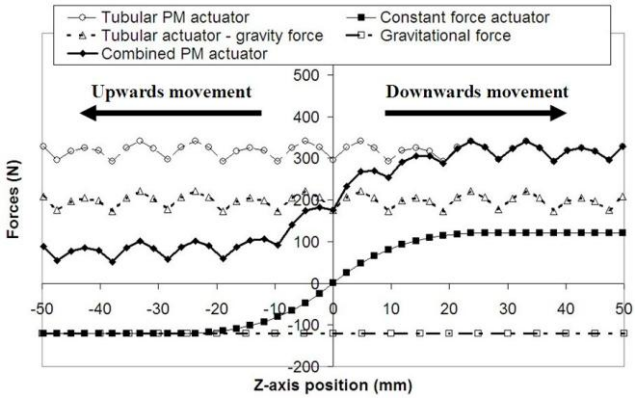

Fig. 11. Combined tubular permanent magnet with constant force actuator: force versus z-axis position characteristic.

6. Conclusions

Several aspects regarding the design of a long stroke actuator that can compensate for translator and nozzle mass in a tubular permanent magnet actuator have been discussed. First the application has been discussed, where clearly the highest dynamical capability for a predetermined volumetric envelope is needed. As such, a slotted tubular PM machine and constant force actuator for 300 N and 120 N have been designed considering electromagnetic and thermal aspects, for which an optimization routine based on the space mapping idea is considered.

The uniqueness of the optimization approach allows the passive constant force actuator to be optimized using just a single analytical equation as a coarse model and extended 3D finite element analyses as a fine model. This actuator exhibits a constant force characteristic (120 N) of approximately 90% of the stroke (z-axis position). Further,

it has been shown that the constant force decreased with increasing number of poles, where the outer radius has to increase by 25% when increasing from 4 to 10 poles.

Finally, this paper showed that the combined actuator produces the required force for the stroke of 50 mm in a single (downwards) z-axis direction.

Acknowledgements

This work was supported by the Assembléon Netherlands B.V., De Run 1102, 5503 LA Veldhoven

References

[1] G J.L. Horijon, Patent US2007/0229851, "Component placement unit as well as a component device comprising such a component placement unit", (2007).

[2] M. Ayob and G. Kendall, "A triple objective function with a Chebychev dynamic pick-and-place point specification approach to optimise the surface mount placement machine", European Journal of Oper. Research, Volume 164, (2005) pp. 609-626.

[3] J.J.H. Paulides, L. Encica, J.W. Jansen, R.A.J. van der Burg, J.L. Horijon, E. Lomonova, "Robot Architecture for a Contactless Industrial Pick-and-Place Machine", Proc. 11th Int. Conf. on Electrical Machines and Systems. Wuhan, China, (2008) pp. 1-6.

[4] K.J. Meessen, B. Gysen, J.J.H. Paulides, E.A. Lomonova, "Halbach Permanent Magnet Shape Selection for Slotless Tubular Actuators", IEEE Trans. on Magnetics, Volume 44, Issue 11, (2008) pp. 4305-4308.

[5] J. Wang, G. W. Jewell, and D. Howe, "A general framework for the analysis and design of tubular linear permanent magnet machines," IEEE Trans. on Magne., Volume 35, no. 3, (1999) pp. 1986-2000.

[6] B.L.J. Gysen, E.A. Lomonova, J.J.H. Paulides, A.J.A. Vandenput, "Analytical and Numerical Techniques for Solving Laplace and Poisson Equations in a Tubular Permanent-Magnet Actuator: Part I. Semi-Analytical Framework", IEEE Trans. on Magn., Volume 44, (2008) pp. 1751 - 1760.

[7] B.L.J. Gysen, E.A. Lomonova, J.J.H. Paulides, A.J.A. Vandenput, "Analytical and Numerical Techniques for Solving Laplace and Poisson Equations in a Tubular Permanent Magnet Actuator: Part II. Schwarz-Christoffel Mapping", IEEE Trans. on Magn., Volume 44, (2008) pp. 1761-1767.

[8] J.L.G. Janssen, J.J.H. Paulides, E.A. Lomonova, "Study of magnetic gravity compensator topologies using an abstraction in the analytical interaction equations". Progress in Electromagnetics Research PIER, 128, (2012) pp. 75-90.

[9] K.J. Meessen, J.J.H. Paulides, E.A. Lomonova, "Modeling of magnetization patterns for 2-DoF rotary-linear actuators" COMPEL: The International Journal for Computation and Mathematics in Electrical and Electronic Engineering, 31(5), (2012) pp. 1428-1440.

[10] K.J. Meessen, J.J.H. Paulides, E.A. Lomonova, "Analysis of a novel magnetization pattern for 2-DoF rotary-linear actuators". IEEE Transactions on Magnetics, 48(11), (2012) pp. 3867-3870.

[11] K.J. Meessen, B.L.J. Gysen, J.J.H. Paulides, E.A. Lomonova, "General formulation of fringing fields in 3D cylindrical structures using fourier analysis. IEEE Transactions on Magnetics", 48(8), (2012) pp. 2307-2323.

[12] J.W. Bandler, Q.S. Cheng, S.A. Dakroury, A.S. Mohamed, M.H. Bakr, K. Madsen, and J. Søndergaard, "Space mapping: the state of the art", IEEE Trans .Microwave Theory Tech., Volume 52, (2004) pp. 337-361.

[13] J. W. Bandler, Q. S. Cheng, D. H. Gebre-Mariam, K. Madsen, F. Pedersen, and J. Søndergaard, "EM-based surrogate modeling and design exploiting implicit, frequency and output space mappings", IEEE MTT-S Int. Microwave Symp. Dig., (2003) pp. 1003-1006.

[14] L. Encica, J.J.H. Paulides, E.A. Lomonova, A.J.A. Vandenput, "Electromagnetic and Thermal Design of a Linear Actuator Using Output Polynomial Space Mapping", IEEE Trans. on Ind. Appl., Volume 44, (2008) pp. 534-542.

[15] L. Encica, J.J.H. Paulides, E.A. Lomonova, "Passive and active constant force-displacement characteristics and optimization of a long-stroke linear actuator", 11th International Conference on Optimization of Electrical and Electronic Equipment, OPTIM 2008. 22-24 May 2008 (2008) pp. 117 - 124.

[16] J.J.H. Paulides, J.L.G. Janssen, L. Encica and E.A. Lomonova, "Tubular permanent magnet actuators: cogging forces characterization", Eurocon, (2009) pp. 1-7.

[17] L. Encica, J.J.H. Paulides, E.A. Lomonova, A.J.A. Vandenput, "Aggressive Output Space-Mapping Optimization for Electromagnetic Actuators", IEEE Trans. on Magnetics, Volume 44, Issue 6, (2008) pp. 1106 - 1109.

[18] L. Encica, "Space-mapping optimization applied to the design of a novel electromagnetic actuator for active suspension", PhD thesis Eindhoven University of Technology, (2008) pp. 1-201.

J.J.H. Paulides (IEEE M'03-SM'13) received the B.Eng. degree from the Avans University, Netherlands, in 1998 and the M.Phil. and Ph.D. degrees in electrical and electronic engineering from The University of Sheffield, Sheffield, U.K., in 2000 and 2005, respectively. Since 2005, he has been a Research Associate and since 2009, he holds a part-time assistant professor position with Eindhoven University of Technology, Eindhoven, Netherlands. Simultaneously he is the CEO of the AE-group within the Netherlands. His research activities span all facets of electrical machines, particularly energy dense linear and rotating machines for automotive and high-precision applications.

L.E. Encica was born in Bucharest, Romania, in 1978. He received the Dipl. Eng. Degree from the University "Politehnica" of Bucharest, Romania, in 2002, and the PhD degree from the Eindhoven University of Technology, Eindhoven, The Netherlands, in 2008. He is currently a CTO within Advanced Electromagnetics BV, Sprang-Capelle, The Netherlands. His research interests are in computer assisted analysis, design and optimization of electromagnetic actuators, motors and sensors.

K.J. Meessen received his BSc, MSc and PhD degree from Eindhoven University of Technology, The Netherlands, in 2012, in the group of Electromechanics and Power Electronics. Simultaneously he is very active within midsize robocup (www.techunited.nl/). Currently he is working within Prodrive BV in Son. His research interests are in robotics, modeling, analysis, as well as design of high-performance electromagnetic actuators.

E.A. Lomonova (IEEE M'04-SM'07-F'10) was born in Moscow, Russia. She received the MSc (cum laude) and PhD (cum laude) degrees in Electromechanical Engineering from the Moscow State Aviation Institute, in 1982 and 1993, respectively. She is currently a Professor with the Department of Electrical Engineering, Eindhoven University of Technology, Eindhoven, The Netherlands. She has worked on electromechanical actuator design, optimization, and the development and realization of advanced mechatronics systems.